Invited Paper

Low-voltage driven graphene-loaded metal wire grating device in total internal reflection geometry for broadband THz modulation

Xudong Liu, Hao Chen, Teng Li, and Yiwen Sun *
Department of Biomedical Engineering, School of Medicine, Shenzhen University, Shenzhen 518060, China
* Email: ywsun@szu.edu.cu

(Received June 2021)

Abstract: Terahertz modulators with capability of both intensity and phase are essential for THz imaging and communication systems. The low-voltage driven THz modulation technique is crucial for integrating the modulators with electronics components. There is still a lack of broadband devices able to achieve both amplitude and phase modulation with low voltage, due to the underlying physics behind existing approaches. Here, we demonstrate a graphene-loaded metal wire grating THz modulator in the total internal reflection geometry to achieve intensity modulation of 80% and phase modulation of 70 degree within 3 volts gate voltage. Quite different from using the strategy of metamaterials based on the electromagnetic resonance effects, our design has performed a broadband modulation for over 1 *THz* bandwidth.

Keywords: Terahertz, Graphene, Metal wire grating, Broadband modulation

doi: 10.1051/tst/2021142044

1. Introduction

In the past decade, terahertz (THz) technology has shown its potential in many areas, e.g. biomedical imaging [1-3], material characterization [4-6] and high-speed wireless communications etc. [7, 8]. Rapid progress made in these applications has deepened our understanding of the significance of THz modulators, which are the crucial components in various microelectronic and photoelectric system. It is still a great challenge to modulate THz signal to achieve both high modulation depth (MD) and broadband response with a single device. The state-of-the-art THz modulator can only work in a narrow bandwidth, which is limited by the narrow band resonance effects [9-11].

Graphene, as its conductivity can be tuned by an external voltage, is heralded as one of the extremely important 2D materials in optoelectronic devices [12], so it has attracted great attention in the THz region [13, 14]. By changing the Fermi level of graphene, its conductivity is able to be tuned from comparatively high-resistance state to semi-metal state. The first demonstration of graphene-based THz modulator was report by Rodriguez *et al*., which achieved a ~15% intensity

modulation [15]. In order to improve the MD of graphene-based modulators, metamaterial structures were widely applied [16-18], but only by narrowing the operational bandwidth. To fully utilize the bandwidth resource of the THz region, a broadband THz modulator is highly desired. In our previse work, the total internal reflection (TIR) geometry and subwavelength metal wire grating were integrated to improve the MD of graphene device from 40% [19] to 77% [20], and still maintaining its operational bandwidth. The TIR geometry ensures a strong interaction between the graphene layer and the evanescent wave of the reflected THz signal; the subwavelength metal wire grating further intensified the THz evanescent electric field in its gaps for an even stronger interaction. Be different to the metasurface, which can only work in a narrow band, the subwavelength metal wire grating is based on a non-resonant electric field enhancement effect, thus the introducing little influence on the operation bandwidth [21]. However, our previous graphene device [20] required a high driving voltage of 60 volts, which limited its integration with the current electronic control system for THz compressive sensing imaging [22, 23].

Here, we demonstrate a new graphene device, using high-κ material Al_2O_3 [24] as the insulation layer (instead of the ordinary material SiO_2), which lowers the gate voltage to 3 volts. The subwavelength metal wire grating is improved from a 30-10μm [20] grating to a 20-4μm grating, which improvs the MD to ~80%. A 72 degrees phase modulation is also achieved in our device, which indicates our design is capable of modulating the amplitude and phase of the THz signal in a broadband at the same time.

2. Experimental methods

A 120-degree high-resistance Si (HR-Si) prism was used to provide a 30 degrees super critical incident angle at the surface of metal grating/air (as shown in Fig. 1 (b)). The polarization of the incident THz light is out-of-paper, which is perpendicular to the metal wire grating (Fig. 1(c)). A 10 *nm*-thick Al_2O_3 layer was grown by ALD process on a HR-Si substrate (square resistivity > 6 $K\Omega \cdot cm$, double side polished). A 5×5 *mm* size metal wire grating was fabricated on the Al_2O_3/Si substrate with standard photolithograph technique and metalized with 5 *nm* thick Ti and 200 *nm* thick gold with period of 20 μm and gap width of 4 μm (abbreviated as 20-4 device in this paper, as shown in Fig. 1(d)). Afterwards, graphene (5×5 *mm*), with sheet resistance around 500 Ω, was transferred on the metal grating. The gate voltage between graphene and HR-Si was swept from -3 *V* to 3 *V*. The transmitted THz time-domain signal was measured by a THz time-domain spectroscopy (TDS) system from TeraView Ltd. (TeraPulse 4000) and the total internal reflection time-domain signal was measured by a modified THz TDS system from Menlo Systems (TERA-K15). The MD of the devices in this paper is defined in the frequency domain with the equation: $MD = \left(1 - E_V^2 / E_{\max}^2\right) \times 100\%$ (Eq.1), where E_V denotes the frequency-dependent amplitude of the measured THz waves under a gate voltage; E_{max} denotes the maximum amplitude of the measured THz waves.

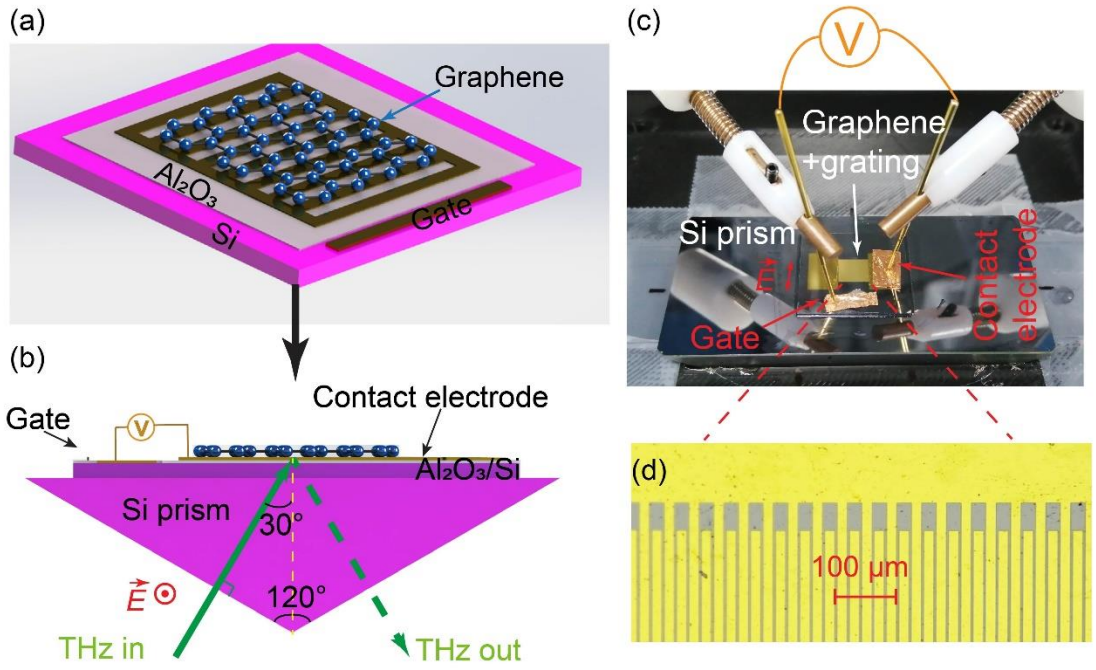

Fig. 1 Device configuration and experiment photos. (a) Schematic illustration of the Al_2O_3/Si gated graphene-loaded metal wire grating device. (b) Side view of the device on a 120 degree high-resistance Si prism and a 30 degree super critical incident angle at the surface of metal grating/air. The polarization of the THz light is out-of-paper. (c) Experimental setup of the TIR measurement. A 5×5 *mm* size graphene is transferred to the metal grating surface. The gate voltage between graphene and HR-Si was swept from -3 V to 3 V. (d) The photo of graphene metal wire grating on Al_2O_3/Si substrate. The period of the metal wire grating is 20 μm and gap width is 4 μm.

3. Results and discussions

The Al_2O_3/Si gated device was measured in the transmission configuration to calculate its MD first; the polarization of the incident THz light was perpendicular to the metal wire grating (Fig. 2(a)). The time-domain signal in transmission geometry decreases gradually as the applied gate voltage tuned from -3 *V* to 3 *V*, which indicates the conductivity of graphene is increased. The time-domain signal is horizontally shifted in optical delay axes for clarity (Fig. 2(b)). The measured THz time-domain waveforms were first truncated to eliminate the effects of multiple reflections within the HR-Si substrate and then Fourier transformed (Fig. 2(c)). The transmitted THz signal under the gate voltage of 3 *V* was selected as the baseline to calculate the MD of the 20-4 device by Eq.1. As shown in Fig. 2(d), the MD gradually increases with the applied gate voltage sweeping from -1 *V* to 3 *V* and reaches its maximum of 20% in a broad bandwidth from 0.5 to 1 *THz*. The MD decreases slightly from 20% at 1 *THz* to 13% at 2 *THz*, which can be explained as the Drude-like frequency dependence of the conductivity of graphene in the THz regime.

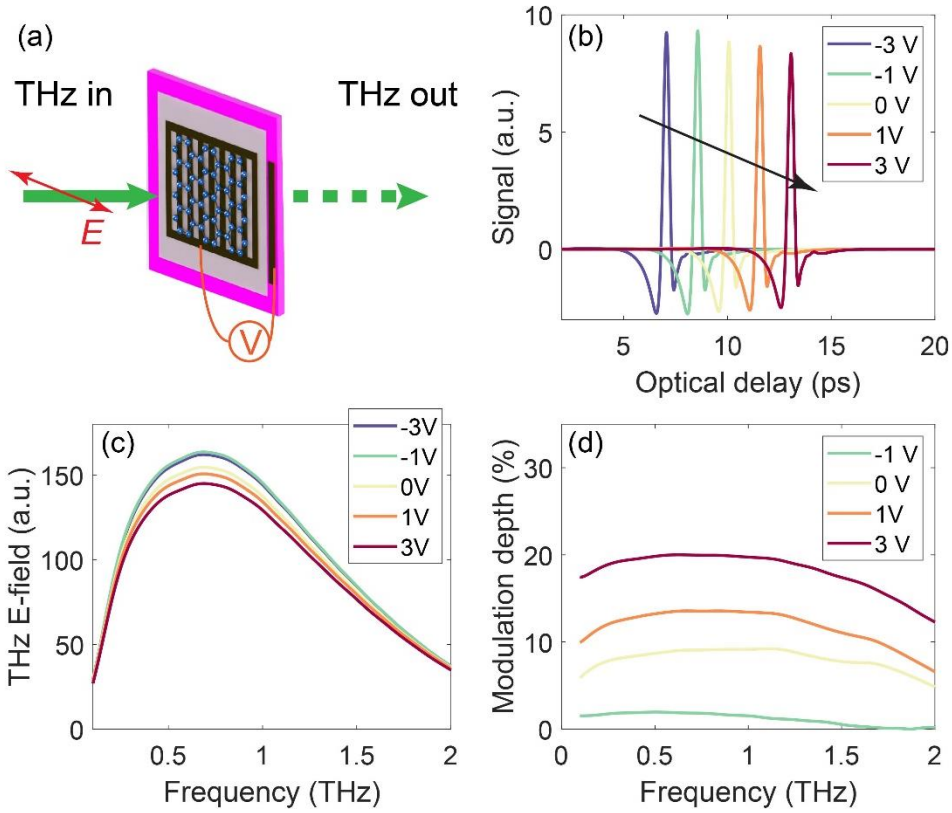

Fig. 2 The experimental configuration and results in transmission geometry. (a) The 20-4 device measured in transmission geometry. (b) The transmitted time-domain THz signal under different gate voltages. The time-domain signal is horizontally shifted in optical delay axes for clarity. (c) The corresponding frequency-domain THz signal and the calculated modulation depth (d).

The 20% MD is insufficient to meet the need of THz modulation, thus a new approach to improve the MD of the device is required, while maintaining its operation bandwidth. Our previous study, by placing the same device in the TIR geometry instead of in the transmission geometry, has shown its capability of increasing the MD in a broadband [20]. Therefore, the 20-4 device was selected and placed on the top surface of the HR-Si prism (Fig. 1(c)) in this work, with the gate voltage swept from -3 *V* to 3 *V*. The amplitude of totally reflected THz signal decreases as the applied voltage swept from -3 *V* to 1 *V*. Compared with the THz waveforms in the transmission geometry, the TIR geometry performed a more efficient modulation to the THz signal. The Fourier transformed THz signal was shown in Fig. 3(b), which has an obvious difference in amplitude. The corresponding MD was calculated and shown in Fig. 3 (c). The deepest MD of the 20-4 device is over 80% at the gate voltage of 1 *V* in the frequency range of 0.4 to 0.57 *THz*. The averaged MD of the 20-4 device in the frequency range of 0.4 to 1.5 *THz* is over 60%. It is worth to notice the amplitude of the totally reflected THz signal increases slightly at 3 *V* and shows a drop around f= 0.5 *THz* in the frequency-domain (Fig. 3(b)). It can be explained with our reported equation in Ref. [20]. The non-resonant electric field enhancement ratio (η) of the metal wire

grating is calculated as grating period (P) divided by gap width (g), thus in the 20-4 device $\eta=P/g=20/4=5$. The theoretical relationship between the reflected intensity and the sheet conductivity, with/out metal wire grating (η=5), is shown in Fig. 3 (d). When the conductivity of the Si/air interface increases from 0 to infinite, the reflected intensity decreases from unit to a minimum value then increases gradually (Fig. 3 (d), blue solid line). When the sheet conductivity of the interface is 0, the incident THz signal is totally reflected by the dielectric interface ("dielectric-like-reflection"); when the sheet conductivity of the interface is close to infinite, the interface performs as a "perfect conductor", and the reflected intensity is also close to unit ("metallic-like-reflection"). The reflection from the interface of prism can be transferred from a "dielectric-like-reflection" to a "metallic-like-reflection" by increasing the conductivity of graphene to a particular sheet conductivity value ("D-M transition point"). In the case of this work, when the sheet conductivity of graphene is around 1.75 *mS* ("D-M transition point"), the reflected THz signal reaches its minimum. When the sheet conductivity of the graphene is tuned higher, the interface shows more "metallic-like-reflection" than the "dielectric-like-reflection". As the conductivity of the graphene is tuned to ~1.75 *mS* under the corresponding gate voltage, the reflected intensity reaches its minimum value (as shown in Fig. 3 (d), green line).

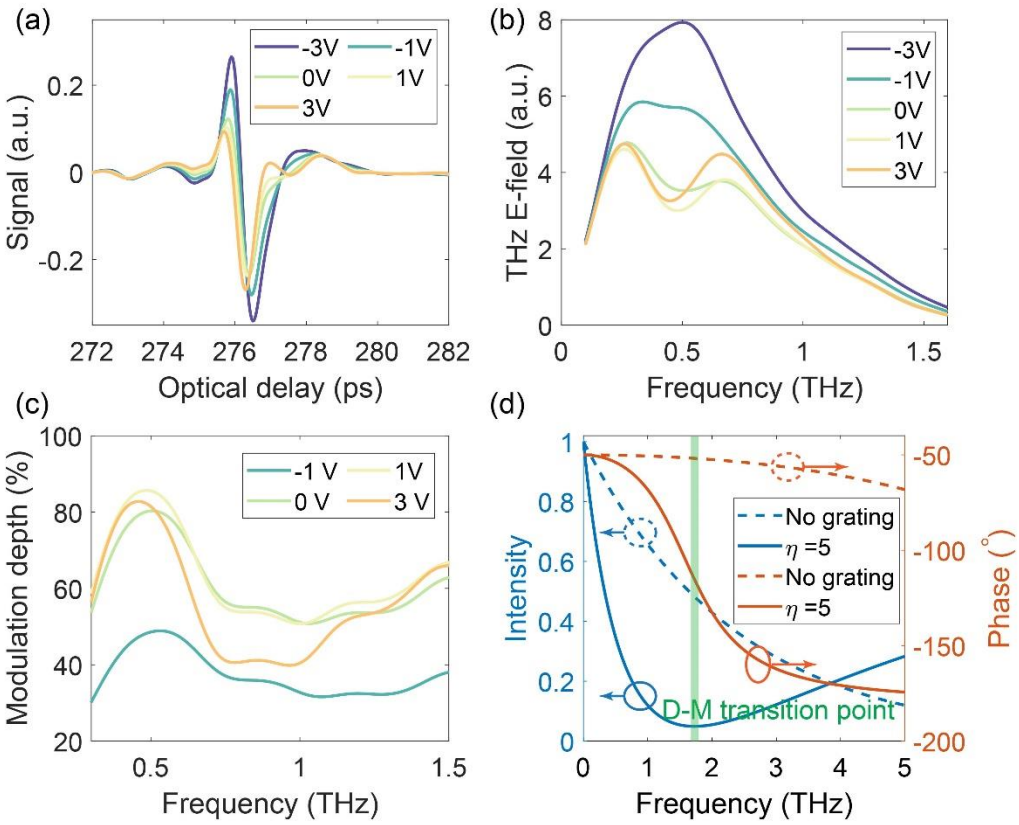

Fig. 3 The experimental results in the TIR geometry. The reflected THz waveforms in time-domain (a) and frequency-domain (b) under different gate voltages. (c) The calculated corresponding modulation depth. (d) The theoretical results of intensity and phase in reflected THz signal with/out metal wire grating.

According to the "D-M transition point" theory, there is a rapid phase change in the reflected

THz signal (Fig. 3(d), orange solid line). The experimental phase information in the frequency-domain is extracted from the time-domain signal by Fourier transform (as shown in Fig. 4). As the gate voltage tuned from 3 *V* to -3 *V*, referenced to the phase at the gate voltage of 3 *V*, the relative phase shift increases monotonically with a modulation range over 70°. The averaged phased shift in the frequency range from 0.4 to 1.5 *THz* is ~60° indicating an ultra-broadband phase modulation is achieved, which is highly consistent with our theoretical predictions. We also noticed there was a relatively larger phase modulation range at lower frequencies (e.g., -72° at 0.57 *THz*) and a relatively smaller phase modulation range at higher frequencies (e.g., 53° at 1.4 *THz*). This frequency dependency is also expected to contribute to the frequency dependent imaginary conductivity of graphene described by the Drude model.

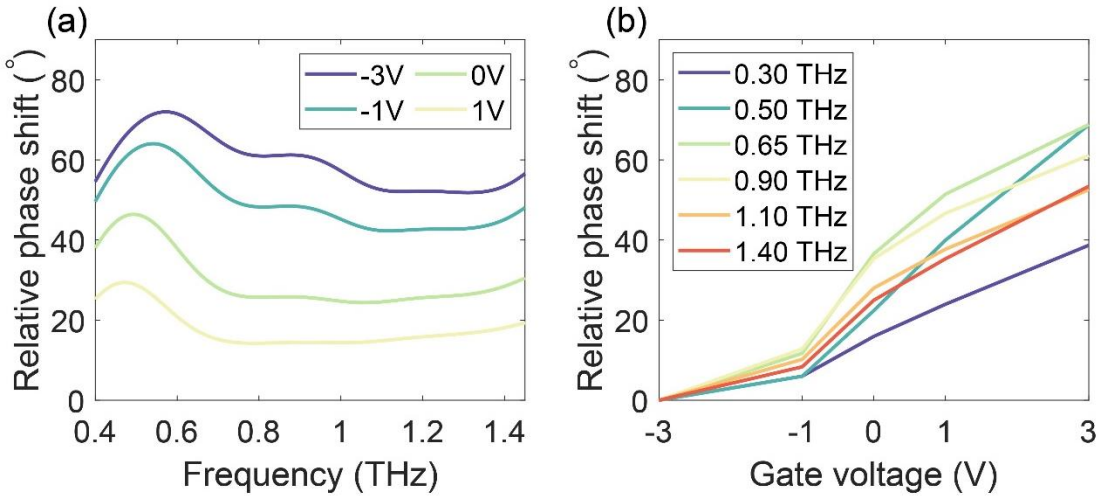

Fig. 4 The 20-4 device worked as a phase modulator under different gate voltages. (a) Relative phase shift referenced to the phase at the gate voltage of 3 *V* from 0.4 to 1.4 *THz*. (b) Phase shift as a function of gate voltage at different frequencies.

The amplitude and phase modulation of our design can be further increased by following methods. Firstly, one could improve the quality of the insulation Al_2O_3 layer. Secondly, a higher quality graphene can be used with less defects. Thirdly, the parameters of the metal grating can be optimized. The modulation speed of this design was limited by the device size and architecture rather than by any intrinsic physical properties of the material. The current device is large due to its being a proof-of-concept hence it is slow, thus future work will look into optimizing the speed of the device as well as having smaller and more desirable sized graphene areas.

4. Conclusions

In this work, a low voltage driven THz amplitude and phase modulator based on graphene-loaded metal wire grating was experimentally demonstrated. The device was fabricated

using a high-κ material Al_2O_3 as the insulation layer, which lowered the operation voltage to 3 volts. Based on this device, a broadband THz intensity modulator with a MD larger than 80% and a broadband phase modulator with a tunability higher than 70 °were demonstrated at room temperature. Our device suggests that there exists a great potential to integrate this design with electronic microcontroller for large-scale THz modulator array control.

Acknowledgments

The authors gratefully acknowledge partial financial support for this work from the National Natural Science Foundation of China [grant numbers 61975135, 61805148], International Cooperation and Exchanges NSFC [grant number 61911530218], Shenzhen International Scientific and Technological Cooperation Project [grant number GJHZ20190822095407131] and Natural Science Foundation of Guangdong Province [grant number 2019A1515010869], Guangdong Medical Science and Technology Research Fund [grant number A2020401], Shenzhen University New Researcher Startup Funding [grant number 2019134, RC00058].

References

[1] S. Fan, B. S. Y. Ung, E. P. J. Parrott, et al.. "In vivo terahertz reflection imaging of human scars during and after the healing process". *J. Biophotonics,* 10, 1143-1151 (2017).

[2] Q. Sun, K. Liu, X. Chen, et al.. "Utilizing multilayer structures to enhance terahertz characterization of thin films ranging from aqueous solutions to histology slides". *Opt. Lett.,* 44, 2149-2152 (2019).

[3] J. D. Buron. "Graphene mobility mapping". *Sci. Rep.,* 5, 1-7 (2015).

[4] Q. Sun. "Highly Sensitive Terahertz Thin-Film Total Internal Reflection Spectroscopy Reveals in Situ Photoinduced Structural Changes in Methylammonium Lead Halide Perovskites". *J. Phys. Chem. C,* 122, 17552-17558 (2018).

[5] S. Fan, M. T. Ruggiero, Z. Song, et al.. "Correlation between saturated fatty acid chain-length and intermolecular forces determined with terahertz spectroscopy". *Chemi. Commun.,* 55, 3670-3673 (2019).

[6] D. Markl. "Analysis of 3D Prints by X-ray Computed Microtomography and Terahertz Pulsed Imaging". *Pharm. Res.,* 34, 1037-1052 (2017).

[7] T. Nagatsuma, G. Ducournau, and C. C. Renaud. "Advances in terahertz communications accelerated by photonics". *Nat. Photon.,* 10, 371-379 (2016).

[8] Y. Zhang. "Gbps Terahertz External Modulator Based on a Composite Metamaterial with a Double-Channel Heterostructure". *Nano Lett.,* 15, 3501-3506 (2015).

[9] Y. Zhao. "Dynamic Photoinduced Controlling of the Large Phase Shift of Terahertz Waves via Vanadium Dioxide Coupling Nanostructures". *ACS Photonics,* 5, 3040-3050 (2018).

[10] Y. Zhao. "High-Speed Efficient Terahertz Modulation Based on Tunable Collective-Individual State Conversion within an Active 3 nm Two-Dimensional Electron Gas Metasurface". *Nano Lett.,* 19, 7588-7597 (2019).

[11] S. J. Kindness. "A Terahertz Chiral Metamaterial Modulator". *Adv. Opt. Mater.,* 8, 2000581 (2020).

[12] K. S. Novoselov. "Electric field effect in atomically thin carbon films". *Science,* 306, 666-669 (2004).

[13] P. Tassin, T. Koschny, and C. M. Soukoulis. "Graphene for terahertz applications". *Science,* 341, 620-621 (2013).

[14] N. Rouhi. "Terahertz graphene optics". *Nano Res.,* 5, 667-678 (2012).

[15] B. Sensale-Rodriguez. "Broadband graphene terahertz modulators enabled by intraband transitions". *Nat. commun.,* 3, 780-787 (2012).

[16] W. Gao. "High-contrast terahertz wave modulation by gated graphene enhanced by extraordinary transmission through ring apertures". *Nano Lett.,* 14, 1242-1248 (2014).

[17] R. Degl'Innocenti. "Fast modulation of terahertz quantum cascade lasers using graphene loaded plasmonic antennas". *ACS Photonics,* 3, 464-470 (2016).

[18] R. Degl'Innocenti. "Low-bias terahertz amplitude modulator based on split-ring resonators and graphene". *ACS Nano,* 8, 2548-2554 (2014).

[19] X. Liu, Z. Chen, E. P. Parrott, et al.. "Graphene based terahertz light modulator in total internal reflection geometry". *Adv. Opt. Mater.,* 5, 1600697 (2017).

[20] Y. Sun. "Graphene-loaded metal wire grating for deep and broadband THz modulation in total internal reflection geometry". *Photon. Res.,* 6, 1151-1157 (2018).

[21] A. Novitsky, A. M. Ivinskaya, M. Zalkovskij, et al.. "Non-resonant terahertz field enhancement in periodically arranged nanoslits". *J. Appl. Phys.,* 112, 074318 (2012).

[22] C. M. Watts. "Terahertz compressive imaging with metamaterial spatial light modulators". *Nat. Photon.,* 8, 605-609 (2014).

[23] B. Sensale-Rodriguez. "Terahertz imaging employing graphene modulator arrays". *Opt. Express,* 21, 2324-2330 (2013).

[24] B. Lee. "Characteristics of high-k Al2O3 dielectric using ozone-based atomic layer deposition for dual-gated graphene devices". *Appl. Phys. Lett.,* 97, 3107 (2010).